

See discussions, stats, and author profiles for this publication at: <https://www.researchgate.net/publication/280032095>

Molecular Dynamics Study of the Gold/Ionic Liquids Interface

ARTICLE *in* THE JOURNAL OF PHYSICAL CHEMISTRY B · JUNE 2015

Impact Factor: 3.3 · DOI: 10.1021/acs.jpcb.5b04505 · Source: PubMed

CITATION

1

READS

39

4 AUTHORS, INCLUDING:



[Carlos Pereira](#)

University of Porto

108 PUBLICATIONS 1,543 CITATIONS

[SEE PROFILE](#)



[Natália D. S. Cordeiro](#)

University of Porto

245 PUBLICATIONS 3,049 CITATIONS

[SEE PROFILE](#)



[Daniel J. V. A. dos Santos](#)

University of Lisbon

52 PUBLICATIONS 354 CITATIONS

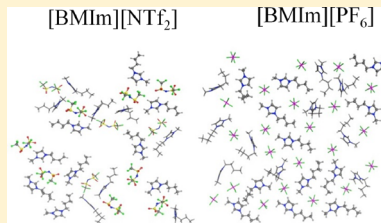
[SEE PROFILE](#)

Molecular Dynamics Study of the Gold/Ionic Liquids Interface

Elisabete S. C. Ferreira,^{†,‡} Carlos M. Pereira,^{*,†} M. Natália D. S. Cordeiro,^{*,†} and Daniel J. V. A. dos Santos^{*,†}

[†]LAQV@REQUIMTE/[‡]CIQUP, Department of Chemistry and Biochemistry, Faculty of Sciences, University of Porto, Rua do Campo Alegre, 4169-007 Porto, Portugal

ABSTRACT: The results of a systematic molecular dynamics study of the interfacial structure between the gold (100) surface and two room-temperature ionic liquids, namely, 1-butyl-3-methylimidazolium hexafluorophosphate ($[BMIm][PF_6]$) and 1-butyl-3-methylimidazolium bis(trifluoromethylsulfonyl)imide ($[BMIm][NTf_2]$), are herein reported. It is found that near an uncharged surface the IL structure differs from its bulk, having an enhanced density extended until the two first layers. Interfacial layering is clearly observed at the gold surface, with a higher effect for the $[BMIm][NTf_2]$ IL but a higher packing for $[BMIm][PF_6]$. In both ILs the alkyl side chains are oriented parallel to the interface while the imidazolium rings tend to be parallel to the interface in about 60% of the cases. The presence of the interface has a higher impact on the orientation of the cations than on the chemical properties of the counterion. The surface potential drop across the interface is more pronounced toward a negative value for ($[BMIm][PF_6]$) than for ($[BMIm][NTf_2]$), due to relatively larger local density of the anions for ($[BMIm][PF_6]$) near the gold surface.



INTRODUCTION

Room-temperature ionic liquids (ILs) are ionic melts with melting points below 100 °C, comprised mostly by organic ions^{1–3} that may display large structural variations. Ionic liquids have emerged as an active area of research due to their physicochemical properties like negligible vapor pressure at elevated temperatures, nonflammability, large stable potential window, and stability over wide temperature ranges. Indeed, ILs are seen as suitable greener alternatives in a wide variety of applications, ranging from synthesis and separation setups⁴ to gas capture efforts,⁵ including electrochemical devices (e.g., solar and fuel cells, batteries, and electrodeposition).^{6–11} In particular, ILs are promising candidates to act as electrolytes in electrical double-layer capacitors, also called supercapacitors. These applications involve interfacial processes, whose detailed knowledge is a fundamental step toward the optimization of such systems.^{12–16}

Since many phenomena occur at interfaces, the study of interfacial properties of ILs has attracted great attention in recent years. However, due to the buried nature of this interface, it is difficult to probe experimentally these complex systems. Moreover, despite the amount of experimental data available on the differential capacitance of electrode/ILs interfaces,^{17–25} as discussed by Lockett et al.,²² it is still difficult to grasp general trends due to several reasons like the purity of the ionic liquid, the reference electrode stability, the nature of the electrode material, and the methods for extracting capacitance data from electrochemical impedance spectroscopy (EIS) results. Nevertheless the experimental data point to a weak dependence of the differential capacitance on the electrode potential, and the values and shape of the potential-dependent capacitance curves depend on the potential scan direction.^{21,23,24}

Molecular simulations are a valuable tool to understand interfacial processes at a molecular level since they are able to describe with atomistic detail the systems and the respective interfaces.²⁶ Atomistic molecular simulations have been used not only as a tool to study the spatial distribution of ions and their behavior near an interface^{10,12,15,27} but also as a method to directly predict the properties of ionic liquids. This predictive ability is very important since there is a multiplicity of possible combinations between the anion and the cation that can be used to form different ILs, the choice depending on the target physicochemical properties desired for a particular application.^{3,28,29}

A vast number of properties of ILs have been calculated using molecular dynamics (MD) or Monte Carlo (MC) simulations (e.g., liquid structure, density, and enthalpy of vaporization).^{30,31} The studies pointed out that the dynamics of ionic liquids tend to be much slower than conventional molecular ones (thus requiring longer simulation times, larger than 1 ns), with evidence of local heterogeneity although with long-range order.³² Coarse-grained³³ and atomistic³⁴ simulations showed that as the length of alkyl tails increases, nanodomains of polar and nonpolar regions occur in the liquid. These nanometer heterogeneities have been confirmed experimentally by X-ray diffraction³⁵ and Raman-induced Kerr effect spectroscopy,³⁶ the size of these heterogeneous regions being proportional to the alkyl chain length of the cation. Hantal et al.¹² found by MD simulations that a phase separation between vapor/liquid interface induces a strong degree of molecular ordering at the interface of the IL, forming

Received: May 11, 2015

Revised: June 19, 2015

Published: June 23, 2015

alternating layers of nonpolar (alkyl chains) and polar (imidazolium rings and anions) regions. In addition, Wang et al.²⁶ reported spatial heterogeneity in the interfacial region formed between imidazolium-based ILs and graphite, the imidazolium rings with the alkyl chains on cations being preferentially orientated parallel to the surface.

Using a combination of MD and density functional theory (DFT), Qiao et al.¹⁶ studied how the anion size ($[{\text{BMIm}}][\text{Cl}]$ and $[{\text{BMIm}}][\text{PF}_6]$) and the electrode curvature influence the microstructure and capacitance of the electrical double layer (EDL) at the IL/electrode interface. They found that the size of the anions affects the distribution of the $[{\text{BMIm}}]^+$ ions near the electrode. It has been generally accepted that ILs ions near solid surfaces have a layering structure.³⁷ Among the ILs most studied are the alkyl-substituted imidazolium ones, which is the reason why it was the choice for the present study.^{1,3,12,14,16,37,38}

Herein, we report a systematic and comparative MD simulation study of the interfacial structure of the gold/IL interface. Furthermore, a comparison is made between imidazolium-based ILs, 1-butyl-3-methylimidazolium hexafluorophosphate ($[{\text{BMIm}}][\text{PF}_6]$) and 1-butyl-3-methylimidazolium bis(trifluoromethylsulfonyl)imide ($[{\text{BMIm}}][\text{NTf}_2]$).

SIMULATION DETAILS

System Building. A face-centered cubic lattice was first setup using 4000 gold atoms with the help of MOE software.³⁹ The system was then subjected to a steepest descent minimization followed by an isotropic 100 ps NpT simulation, a cubic box with 4.07 nm of side being obtained. This system was then sliced (only in the z direction) to obtain a gold solid slab of $4.07 \times 4.07 \text{ nm}^2$ in the x and y directions and $\sim 2.5 \text{ nm}$ in the z axis.

A pure IL system containing 716 $[{\text{BMIm}}]^+$ and 716 $[\text{PF}_6]^-$ ions was built by increasing the system size through replication of a previously equilibrated in-house system.¹² An NpT run using a Berendsen thermostat and barostat was followed for 200 ps to obtain an interfacial area of about $4.07 \times 4.07 \text{ nm}^2$. Afterward, another NpT run was carried out for 500 ps using a Nose–Hoover thermostat and a Parrinello–Rahman semi-isotropic pressure coupling to keep the interface area fixed.

To obtain a system of pure $[{\text{BMIm}}][\text{NTf}_2]$ with similar size as in the previous $[{\text{BMIm}}][\text{PF}_6]$ system, 512 cations and 512 anions were disposed randomly in a cubic lattice. A steepest descent minimization was first used to relax the system. Then a 1 ns NpT run using the Berendsen thermostat and barostat led to a system with the expected density. Another 1 ns NpT run was used to obtain a system with a similar interfacial area as for the other IL. Another equilibration run was executed over this system for 30 ns using a Nose–Hoover thermostat and a Parrinello–Rahman semi-isotropic pressure coupling while keeping the interfacial area fixed.

To build the final $[{\text{BMIm}}][\text{PF}_6]$ system in contact with the two gold slabs at both ends of the IL, the previously obtained $[{\text{BMIm}}][\text{PF}_6]$ system was duplicated in the z direction and inserted between two similar gold slabs. The slabs were translated in the z direction as needed to obtain the slabs in the right position, and a gap of 4 Å between the different slabs was used to avoid close contacts between atoms. A 50 ps NVT run followed to relax the system, and a 100 ps NpT run was then used to collapse the empty space between the slabs by slowly decreasing the system size in the z axis using a Berendsen thermostat and barostat. For the final equilibration the system

was manipulated to separate the two gold slabs by 5 nm. The system obtained has a length in the z direction of 25 nm that was kept fixed in the following 20 ns NpT equilibration and 50 ns NpT production runs by applying a Nosé–Hoover thermostat and a semi-isotropic Parrinello–Rahman barostat. The system having the $[{\text{BMIm}}][\text{NTf}_2]$ in contact with the two solid gold slabs was obtained in a similar way as described for the $[{\text{BMIm}}][\text{PF}_6]$ system in contact with gold (the final equilibration run was extended to 30 ns) and was already used successfully as the starting point in other simulations.⁴⁰

In this way, two different systems containing $[{\text{BMIm}}][\text{NTf}_2]$ and $[{\text{BMIm}}][\text{PF}_6]$ ionic liquids in contact with two solid gold slabs were obtained having the same fixed length in the z direction of 25 nm and a varying surface area of about $4.07 \times 4.07 \text{ nm}^2$. For both systems, in the z direction, the gold slabs have $\sim 2.5 \text{ nm}$ and the ionic liquids $\sim 15 \text{ nm}$.

Force Field and Simulation Parameters. Heinz et al.⁴¹ developed a parametrization for several face-centered cubic metals via 12-6 Lennard-Jones interactions, and this was the potential used to model the gold interactions. The potential used to model $[{\text{BMIm}}][\text{PF}_6]$ was developed by Lopes et al.⁴² For $[{\text{BMIm}}][\text{NTf}_2]$, a reparameterization by Köddermann et al.⁴³ of the previous force field by Lopes et al.⁴² was used. This improved force field adds a new atom type and different Lennard-Jones parameters in $[{\text{BMIm}}]^+$ and was refined to correctly reproduce both the densities and self-diffusion coefficients although keeping the partial atomic charges unchanged. For the interactions between different atom types the Lorentz–Berthelot mixing rules were applied, as required by the parametrization of the force fields used.

All MD simulations were carried out with the GROMACS simulation package, version 4.6.2,⁴⁴ and followed at 300 K and at a pressure of 1 bar with a time step of 2 fs. Periodic boundary conditions were applied in all directions with long-range van der Waals tail corrections for both energy and pressure applied for distances larger than 1.2 nm. The same cutoff was used for the long-range electrostatic interactions in combination with the particle mesh Ewald technique^{45,46} and for the neighbor list using a Verlet cutoff scheme.

For final equilibration or production runs under constant temperature and pressure, a Nosé–Hoover thermostat^{47,48} with a coupling constant of 1 ps and a Parrinello–Rahman coupling⁴⁹ with a time constant of 5 ps were used. In initial equilibration runs still far from equilibrium, the more robust Berendsen thermostat and barostat were used. In systems containing pure liquids or pure gold, an isotropic pressure coupling was applied while in systems containing interfaces, a semi-isotropic coupling was used in order to decouple fluctuations between the interface and the long MD box z axis (the length in z was fixed, and the interfacial area was allowed to fluctuate with a compressibility of $4.5 \times 10^{-5} \text{ bar}^{-1}$). Only the covalent hydrogen bonds lengths were constrained.

Trajectory data were written at every 2 ps and later analyzed using our own programs (written in C++, and linked with the GROMACS library interface) whenever the respective analysis tool was unavailable in GROMACS.

RESULTS AND DISCUSSION

Table 1 collects the densities for the $[{\text{BMIm}}][\text{PF}_6]$ and $[{\text{BMIm}}][\text{NTf}_2]$ systems, which could be estimated using a slab of 5 nm (z direction) in the bulk IL region and at half way between the two gold interfaces. It also summarizes the total number of ions and gold atoms present in each simulated

Table 1. Total Number of Ions and Gold Atoms in Each of the Simulated Systems and Respective Equilibrium Densities for the Pure Ionic Liquids (Experimental Values inside Parentheses)

system	number of ionic and atomic species			gold	$\rho/\text{g cm}^{-3}$
	[BMIm] ⁺	[NTf ₂] ⁻	[PF ₆] ⁻		
[BMIm] [PF ₆]/gold	716	0	716	5200	1.362 (1.3674 ⁵⁰)
[BMIm] [NTf ₂]/gold	512	512	0	5200	1.410 (1.43 ⁵¹)

system containing IL/gold interfaces. As can be seen, for pure ILs, the bulk densities compare quite well to the experimental values.

The number densities of the ionic species present in [BMIm][PF₆] and in [BMIm][NTf₂] are presented in Figure 1 as a function of the distance to the gold interface. The MD box was divided in 1000 bins, and the number of atoms in each bin was calculated. The average number of atoms in each bin was divided by the number of sites in each ion to obtain the average number of ions in each bin. The resulting value was then averaged using the values obtained through the two interfaces.

As observed by other authors for, e.g., the [BMIm][PF₆]/graphite system,^{52–54} the strong layering capability of the ions in both interfaces can be seen. This layering is especially strong in the first and second layers where the change in density is much larger than beyond this distance. However, in both interfaces the maximum for [BMIm]⁺ is about three times the density of bulk, similar for [PF₆]⁻ but lower for [NTf₂]⁻, and the minimum of this first peak occurs basically at the same distance for all ions at ~5 Å (only slightly shorter for [NTf₂]⁻). Defining this distance as the point where the first layer ends, it is clearly seen by analyzing Figure 1 that [BMIm]⁺ starts to appear closer to the gold interface and that in [BMIm][NTf₂] the [NTf₂]⁻ peak is sharper than [BMIm]⁺, while in the other IL the [BMIm]⁺ peak is sharper than [PF₆]⁻ which means that inside this first layer the cations are more packed in a thinner sheet than the anions in [BMIm][PF₆] while the opposite occurs in the other IL. This first layer has about 4 Å of thickness for [BMIm]⁺ and a little bit less (3.4 Å) for [NTf₂]⁻ and a slightly more for [PF₆]⁻ (4.3 Å).

An interesting observation is that the location of the first cationic layer of [BMIm]⁺ is not affected by the type of anion although the maximum is higher in [BMIm][PF₆] than in

[BMIm][NTf₂], which demonstrates a higher packing in the former. Doing the integration of the curves and the conversion to obtain the number of ions in the first layer in direct contact with gold, in [BMIm][NTf₂] an average of 17.5 ions are found for [BMIm]⁺ and 10.5 for [NTf₂]⁻. In [BMIm][PF₆], the number of ions of each species is even greater; i.e., 21.8 ions are found for [BMIm]⁺ and 21.4 ions for [PF₆]⁻. The higher number of ions found in [BMIm][PF₆] is a reflex of the higher number density in bulk that happens also at the interface, although the much lower number of [NTf₂]⁻ ions must have a diverse origin, namely in the differences also found for the second layer.

A comparison of all ions also shows that the layering effect is higher for the larger [NTf₂]⁻. Especially for this ion, it is the one that extends the most inside the IL disappearing only at distances larger than 4 nm from the interface. Another difference can be found in the first peak for the anion and cation that are both sharp in [BMIm][NTf₂] while in [BMIm][PF₆], although the cation peak is also sharp, for the anion it is divided in three sharp peaks with maxima of 8, 4.8, and 8 giving a ratio of 5/3 between the two different peaks with equal maxima closer and further away from the interface with the smaller peak in between. These peaks are related with three slightly different distances at the interface that the smaller [PF₆]⁻ ion can occupy, the peaks being equally spaced and separated by only 1 Å.

Regarding the second layer, a clear difference is also found between both ILs. While in [BMIm][PF₆] the density fluctuations of [BMIm]⁺ and [PF₆]⁻ appear to be in phase, i.e., when there is an increase in the density of the cation this increase is also followed by the anion, this seems not to be the case in [BMIm][NTf₂] where the maximum of the second peak of [BMIm]⁺ occurs toward the end of the second layer of [NTf₂]⁻. The lower number of [NTf₂]⁻ ions in the first layer seem to be relocated in this second layer with maxima just after the minimum of the first [BMIm]⁺ layer, whereas for [PF₆]⁻, the maximum is located at a much larger distance. Another difference is that for [NTf₂]⁻ the maximum of the second layer is much closer to the value of the maximum of the first peak than in the case of [PF₆]⁻.

For distances larger than the two first layers close to the gold/IL interface, the change of the densities with the distance to the interface exponentially damps to the bulk regime following a behavior that can be characterized by a damped oscillator. Damped oscillations can be described by the following equation:

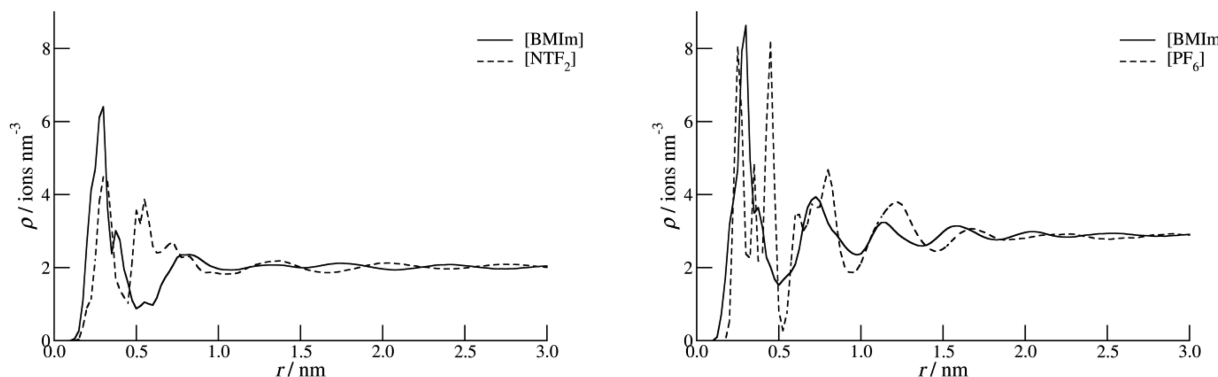


Figure 1. Average number density profiles for [BMIm]⁺ and [NTf₂]⁻ in the gold/[BMIm][NTf₂] system (left) and [BMIm]⁺ and [PF₆]⁻ in the gold/[BMIm][PF₆] system (right), both as a function of the distance to the gold surface.

$$\rho(r) = ae^{-\gamma r} \cos(\omega r + \delta)$$

As an example, a fit to the data using this equation is shown in Figure 2 for the evolution of the $[\text{NTf}_2]^-$ density with the

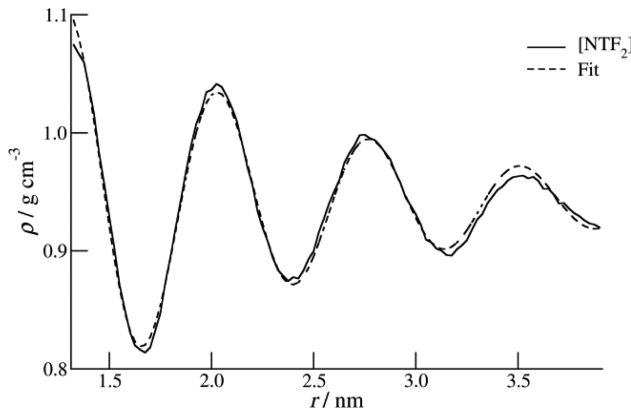


Figure 2. Density profiles for $[\text{NTf}_2]^-$ in the $[\text{BMIm}][\text{NTf}_2]$ ionic liquid as a function of the distance to the gold surface for distances larger than the first two layers closest to the gold/IL interface. A fit to a function describing damped oscillations is also displayed.

distance to the gold/IL interface. A comparison of the parameters resulting from the fitting to the data shows that the frequency ω is higher for the ions in the $[\text{BMIm}][\text{PF}_6]$ IL than for $[\text{BMIm}][\text{NTf}_2]$. This seems to be a consequence of the higher capacity of the $[\text{PF}_6]^-$ ion to pack in more compact layers due to its smaller size when compared to $[\text{NTf}_2]^-$. The parameter γ also shows a higher value in the $[\text{BMIm}][\text{PF}_6]$ ionic liquid which means that the exponential decay is higher in this IL.

Since these systems can be considered a model of an electrochemical experiment with no electrical potential applied at the gold electrodes, it is important to analyze how the electron density varies with the distance to the solid gold interface, as shown in Figure 3. This figure also makes clear the impact of the gold interface in the layering of the ions that, assisted with a particular orientation, can build electrical double layers at this interface. From the global aspect of the two graphs, although the behavior of this property seems to differ between the two systems, the first striking consistency is that the fluctuations in the electron density are governed by the

anions. In both systems, the largest fluctuations occur for $[\text{PF}_6]^-$ and $[\text{NTf}_2]^-$ with a low capability for $[\text{BMIm}]^+$ to shield the excess of local charge due to a specific orientation of the anion. Moreover, although in $[\text{BMIm}][\text{NTf}_2]$ the cation has a region where the local charge density is negative, this never happens in the other system, always being positive.

The organization of the ions is such that at about the same distance in both interfaces ($\sim 2 \text{ \AA}$) a slight excess of positive charge is built by the $[\text{BMIm}]^+$ ions. Then, at a larger distance, the anions generate a local excess of negative charge that is much larger for $[\text{NTf}_2]^-$ than $[\text{PF}_6]^-$ that is followed by a layer of excess positive charge also built by the anions. In this double layer, the layer containing excess of negative charge and the layer that just follows containing an excess of positive charge are, for the two different interfaces, located at the same distance from gold.

After this second electric layer, two more layers mimic the first ones being not as sharp and with lower charge density, especially in the $[\text{BMIm}][\text{NTf}_2]$ case, which are slightly different. That is, in the $[\text{BMIm}][\text{PF}_6]$ IL, there is another layer containing excess of negative charge that is sharp and has higher density than the first negative one, while for $[\text{BMIm}][\text{NTf}_2]$ although there is also a local excess of negative charge, this occurs at a broader distance and with less negative charge density. Also in $[\text{BMIm}][\text{PF}_6]$, it seems that the last positive layer is made of two sublayers with a slight negative plane in between.

Kislenko et al. have studied the $[\text{BMIm}][\text{PF}_6]$ ionic liquid in contact with the basal plane of graphite. The reported charge density fluctuations near the interface are quite similar to the ones found herein. With minor differences in the values of the peaks minima and relative distance to the interface, the global value of the peaks are quite similar, showing that at zero charge the packing of the ions is more dependent on the IL than on the impact of these two interfaces.⁵⁵

It is important to note that the changes in excess of local charges occur in narrow distances. In each layer of the double layer, the charge excess occurs only in a region with less than 1 \AA thickness, and 3 \AA is the distance that goes from the starting of the charge excess to the end of the first double layer. These distances are quite similar between both interfaces. At distances larger than $\sim 10 \text{ \AA}$, the impact of the gold interface is lost and there is no local charge excess.

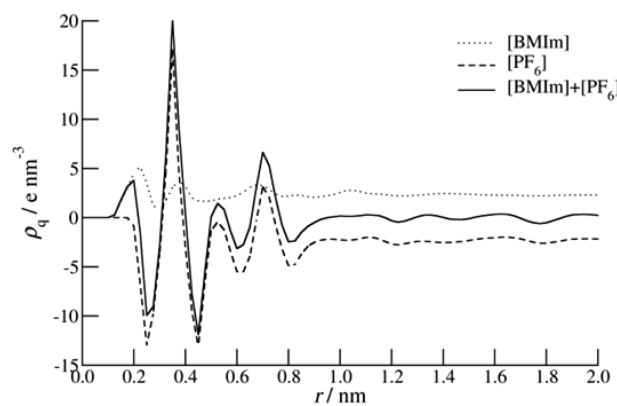
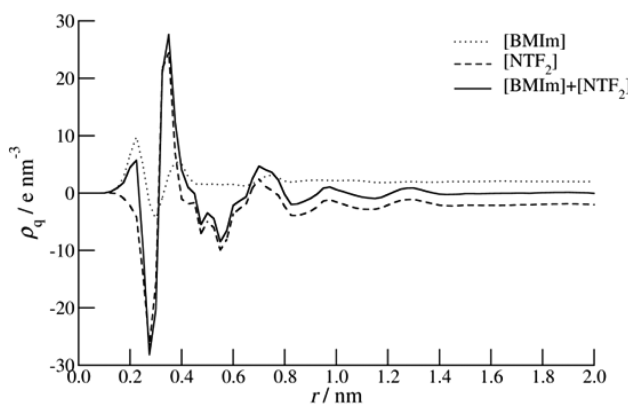


Figure 3. Average electron density for $[\text{BMIm}]^+$ and $[\text{NTf}_2]^-$ in the gold/ $[\text{BMIm}][\text{NTf}_2]$ system (left) and $[\text{BMIm}]^+$ and $[\text{PF}_6]^-$ in the gold/ $[\text{BMIm}][\text{PF}_6]$ system (right), both as a function of the distance to the gold surface. The average of the total electron density for each system is also displayed (solid line).

Local excess of electric charge originates an electric field E that can be calculated by integrating over the local charge density fluctuations along the vector normal to the gold/IL interface inside the IL (ϵ is the vacuum permittivity):^{56,57}

$$E(z) = \epsilon_0^{-1} \int_{\text{IL}} \rho(z) dz$$

The potential drop (potential of zero charge, PZC) can be obtained by integrating the electric field E over the IL also in the direction of the interface normal and is represented in Figure 4 as a function of the distance to the gold/IL interface:

$$\Delta\Phi(z) = - \int_{\text{IL}} E(z) dz$$

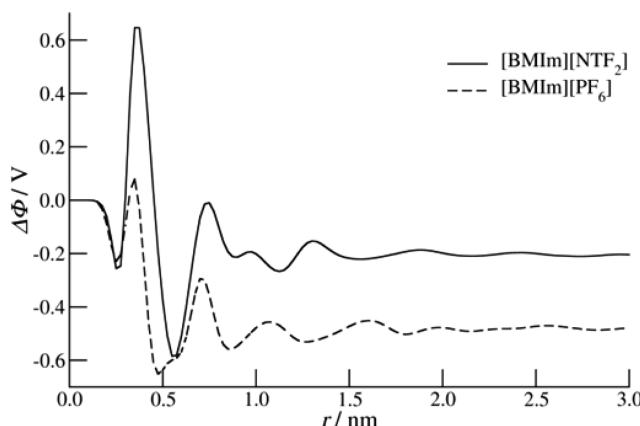


Figure 4. Potential drop along the normal to the gold interface for $[\text{BMIm}][\text{PF}_6]$ and $[\text{BMIm}][\text{NTf}_2]$.

The potential drop across the IL although very different for the two systems is negative in both, which indicates that the anion has a higher affinity toward the uncharged gold surface than the cation. While in $[\text{BMIm}][\text{NTf}_2]$ the potential drop is a little less than half the value for $[\text{BMIm}][\text{PF}_6]$ (about -0.2 V), due to the higher packing capacity of the $[\text{PF}_6]^-$ smaller anion, the initial fluctuations near gold are much larger. This is due to the also larger charge density fluctuations near gold found for $[\text{BMIm}][\text{NTf}_2]$, which have higher relative $[\text{BMIm}]^+$ ions in the first layer (17.5 $[\text{BMIm}]^+$ ions against 10.5 $[\text{NTf}_2]^-$ ions,

while the IL $[\text{BMIm}][\text{PF}_6]$ present, in the first layer, 21.8 ions for $[\text{BMIm}]^+$ and 21.4 ions for $[\text{PF}_6]^-$). Moreover, the second minimum found for the potential drop is closer to the gold interface in $[\text{BMIm}][\text{PF}_6]$ due to the higher packing capability of the $[\text{PF}_6]^-$ anion due to its smaller size.

Vatamnu et al.⁵⁸ calculated, at 393 K, the potential drop for different $[\text{C}_n\text{MIm}][\text{NTf}_2]$ ($n = 2, 4, 6$, and 8) near flat and rough graphite electrodes and have obtained a potential quite similar to the one obtained herein of -0.22 V for $[\text{BMIm}][\text{NTf}_2]$ in contact with the flat interface. Previously, the authors have reported a change of only 0.07 V in the PZC for the *N*-methyl-*N*-propylpyrrolidinium bis(trifluoromethane)sulfonyl imide IL in contact with a graphite interface for temperatures ranging from 363 to 453 K.¹⁵ Cummings and co-workers⁵⁹ have also calculated the potential drop of $[\text{C}_3\text{MIm}][\text{BF}_4]$ near the neutral planar carbon electrode (graphene sheets) at 450 K. The fluctuations in the potential drop profile are lower than the ones herein reported for the gold interface in contact with $[\text{BMIm}][\text{PF}_6]$ or $[\text{BMIm}][\text{NTf}_2]$, and the potential drop obtained was just slightly above -0.2 V.

The excess of local charges in each layer can only be due to ions assuming a particular orientation that concentrates the atoms' partial charges of the same sign at a certain distance to the interface. Therefore, in order to study the orientation of the ions at the gold interface, some vector definitions were made and are represented in Figures 5 and 6 for $[\text{BMIm}]^+$ and $[\text{NTf}_2]^-$, respectively.

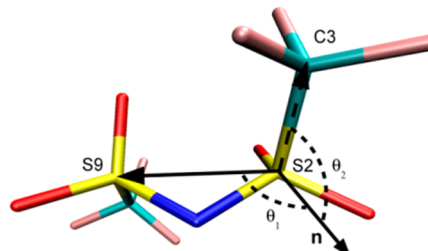


Figure 6. Definitions for the two molecular tilt axes for the $[\text{NTf}_2]^-$ ion. The vector perpendicular to the gold/IL interface plane is the vector \mathbf{n} . Sulfur atoms are displayed in yellow, nitrogens in dark blue, carbons in light blue, fluorine atoms in pink, and oxygens in red.

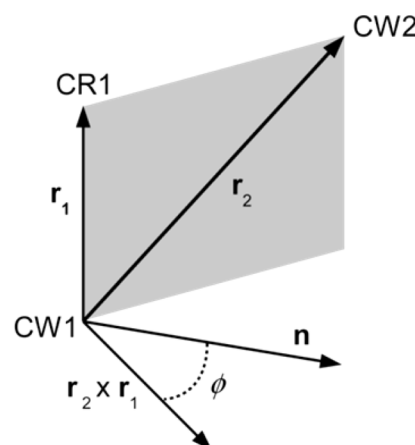
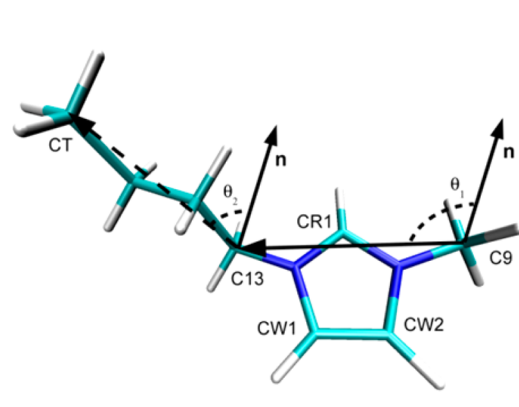


Figure 5. Definitions for the two molecular axes (left) and for the molecular plane axis (right) for the $[\text{BMIm}]^+$ ion. The vector perpendicular to the gold/IL interface plane is the vector \mathbf{n} . In the picture on the left, nitrogen atoms are displayed in dark blue, carbons in light blue, and hydrogens in white.

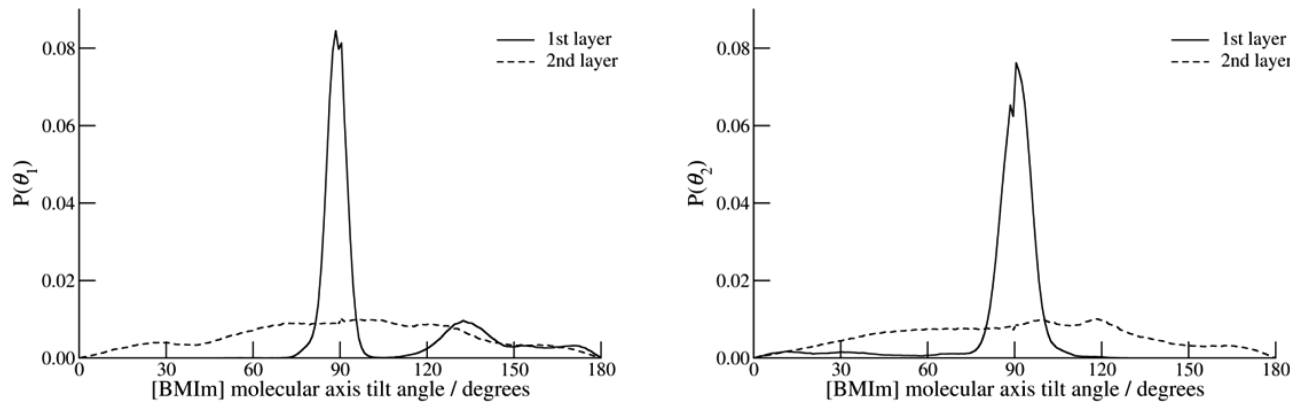


Figure 7. Normalized tilt axis probability distribution for the $[\text{BMIm}]^+$ ions found in the first and second layers in $[\text{BMIm}][\text{NTf}_2]$ as defined by the density profiles found in Figure 1. Left: the tilt angle is defined as the angle between the unit vector axis normal to the gold/IL surface and the longer molecular axis passing through the imidazolium ring (cf. Figure 5). Right: the tilt angle is defined as the angle between the unit vector axis normal to the gold/IL interface and the longer molecular axis of the saturated carbon chain (cf. Figure 5).

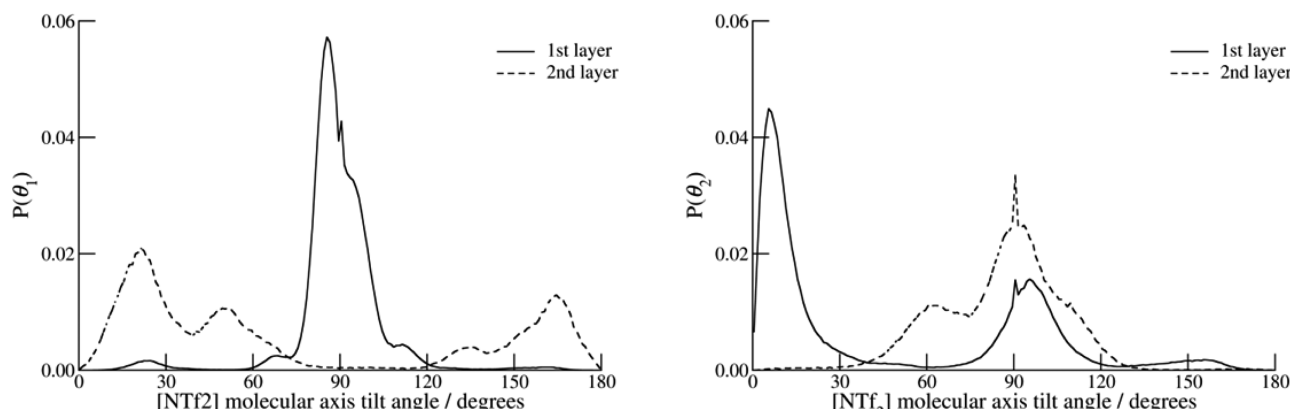


Figure 8. Normalized tilt axis probability distribution for the $[\text{NTf}_2]^-$ ions found in the first and second layers in $[\text{BMIm}][\text{NTf}_2]$ as defined by the density profiles found in Figure 1. Left: the tilt angle is defined as the angle between the unit vector axis normal to the gold/IL interface and the longer molecular axis passing through both sulfur atoms (cf. Figure 6). Right: the tilt angle is defined as the angle between the unit vector axis normal to the gold/IL interface and the longer molecular axis defined by the sulfur and the terminal methyl carbon atoms (cf. Figure 6).

To assess the orientation of the imidazolium ring and of the imidazolium aliphatic carbon chain in relation to the plane of the IL/gold interface, two molecular axes were used (cf. Figure 5). The tilt angle first is defined as the angle between the vector uniting the carbon methyl and methylene groups directly connected to the imidazolium ring and a unit vector in the z direction (this is the vector perpendicular to the gold/IL interface plane), and the other is defined by the angle between the vector uniting both ends of the aliphatic carbon chain and a unit vector in the z direction.

To understand the orientation of the imidazolium ring plane in relation to the IL/gold interface plane, a molecular plane tilt axis was also defined. Using the three carbon atoms of the imidazolium ring (Figure 5, left) two vectors uniting these carbons can be used to define a molecular plane (Figure 5, right). The molecular plane tilt angle is defined as the angle between the vector obtained by the external product of the two molecular plane axes and a unit z vector perpendicular to the IL/gold interfacial plane.

In a similar way, molecular axes were also defined for $[\text{NTf}_2]^-$. One is defined by the two sulfur atoms, and the other is the vector uniting a sulfur atom and the carbon that is directly bonded to it (Figure 6).

For $[\text{PF}_6]^-$ ions, the molecular tilt axis was defined as the angle between the vector uniting two fluorine atoms in

opposite sides of the ion and passing through the central phosphor atom and a unit vector in the z direction. No plane tilt axis was defined since, due to symmetry reasons, the information is the same as for the molecular tilt axis.

A tilt axis can be defined between the gold surface normal and the molecular axes defined above. The instantaneous values can be collected in a discrete vector between 0 and 180°, and the number found for each bin is a tilt axis probability distribution. The molecules of the first and second layer were used in the calculations, and the normalized results for the two $[\text{BMIm}]^+$ tilt axes are presented in Figure 7 for $[\text{BMIm}]^+$ in the $[\text{BMIm}][\text{NTf}_2]$ IL. For $[\text{BMIm}]^+$ in $[\text{BMIm}][\text{PF}_6]$, the probability distributions are quite similar showing that the orientations of molecular axes of the ions have a higher dependency on the interface than on the counterion.

While in the first layer the vectors are strongly oriented toward a 90° tilt (vector parallel to the gold interface), this is basically destroyed in the second layer. This means that in the first layer, both the molecular vectors defined by atoms in the carbon chain and in the imidazolium ring tend to be parallel to the interface. However, a long shoulder exist for angles larger than 110° with a maximum around 130° that is similar to the one found for the vector defined by the carbon chain tilt axis for angles lower than 90°. Since the two vectors are defined for the same molecule, they have a certain correlation that is

demonstrated by these two shoulders. A visual inspection of this first layer shows some $[\text{BMIm}]^+$ ions both with the two vectors parallel to the interface while others have the carbon chain parallel to the interface and the ring protruding toward the second layer. This is the reason for the shoulder in the $[\text{BMIm}]^+$ imidazolium molecular axis with values higher than 90° with a maximum at 130° meaning also that, in this case, the methyl carbon directly connected to the ring is in a position further away from the interface. This picture will become clearer while analyzing the orientation of the imidazolium ring plane.

Although the probability distribution of the peak around 90° is sharper in the case of the molecular axis defined by ring atoms, integration of the curves shows that 73% of angles defined by this vector are lower than 106° (end of the peak) while for the vector defined by the atoms in the carbon chain, 92% of the ions have angles larger than 75° ; i.e., the peak is broader for the carbon chain but more ions tend to have the carbon chain with orientation closer to 90° . The distribution found for $[\text{BMIm}]^+$ in $[\text{BMIm}][\text{PF}_6^-]$ is similar to only a larger tendency for the tilt angle defined by the molecular axis containing the imidazolium atoms to have angles different than 90° (peak accounts for 63%).

The tilt angles distributions for the molecular axes of $[\text{NTf}_2]^-$ are displayed in Figure 8 for the orientations found in the first and second layers. Again, a clear difference is found between the two layers with sharper peaks found in the first layer, but in opposition to $[\text{BMIm}]^+$, the second layer still clearly retains preferential orientations. The molecular tilt axis defined by the vector uniting the two sulfur atoms and the vector normal to the interface has also an orientation preference around 90° meaning that this axis tends to be parallel to the interface. However, in the second layer, this orientation is completely shifted to angles different than 90° , namely, $\sim 20^\circ$, $\sim 50^\circ$, $\sim 130^\circ$, and $\sim 160^\circ$, in which, due to the molecular symmetry, the maximum at 20° is the same as the one at 160° and the same happens for the other two angles.

The other $[\text{NTf}_2]^-$ molecular tilt axis defined using the sulfur and carbon atoms directly connected has a clear preference to be either almost perpendicular or almost parallel to the gold/IL interface (deviation of about 5°). A visual inspection shows that these two orientations are correlated since a typical orientation of $[\text{NTf}_2]^-$ has one $\text{S}-\text{CF}_3$ vector parallel to the interface while the other tends to be perpendicular. A difference found for the distribution of this molecular tilt axis is that, although low, it never goes to zero while away from these two preferred orientations. In the second layer the preferred angle is located only around 90° although much broader than in the first layer and having a shoulder with a maximum at 60° .

The probability distributions of the tilt angle in the first and second layers for $[\text{PF}_6^-]$ have two symmetric maxima one at $\sim 53^\circ$ and the other at $\sim 127^\circ$ that correspond to the same orientation due to the symmetry of the ion (Figure 9). If the angle was 45° , two fluorine atoms would be at the same distance to the interface. This way, there is a preference for one of the fluorine atoms to be in closer contact to gold. A detailed analysis of the three sublayers inside the first layer of $[\text{PF}_6^-]$ described when discussing the number density change with the distance to the gold interface (cf. Figure 1 on the right) showed similar tilt angle distributions in all the sublayers although the first was more discrete indicating that the ions in this layer are very much trapped to particular angles not assuming continuous angle values.

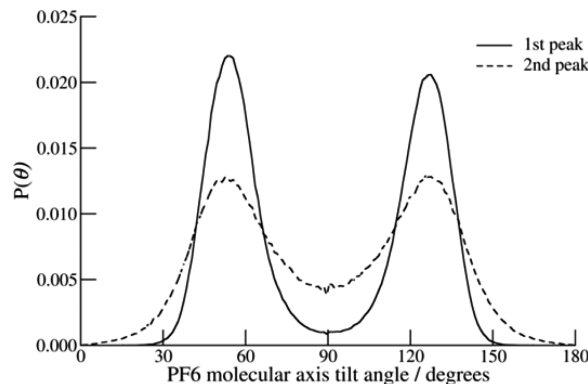


Figure 9. Normalized tilt axis probability distribution for $[\text{PF}_6^-]$ ions in $[\text{BMIm}][\text{PF}_6]$ for the first and second layers as defined by the density profiles found in Figure 1. The tilt angle is defined as the angle between the unit vector axis normal to the gold/IL interface and the longer molecular axis uniting two fluorine atoms and passing through the phosphor.

The tilt of the imidazolium ring plane of $[\text{BMIm}]^+$ was also studied as defined in Figures 5, and the probability distributions are presented in Figure 10. This distribution has three peaks,

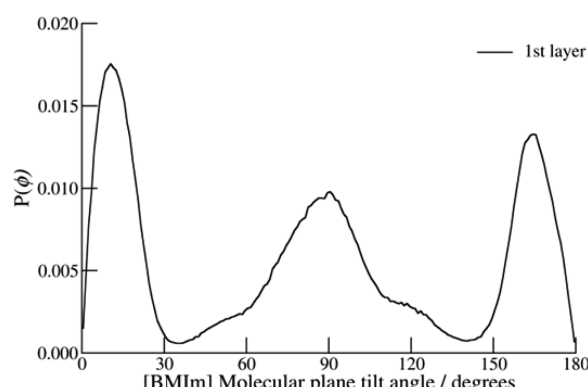


Figure 10. Normalized tilt plane probability distribution for the $[\text{BMIm}]^+$ in $[\text{BMIm}][\text{NTf}_2]$ for the first and second layers as defined by the density profiles found in Figure 1. The tilt angle is defined as the angle between the unit vector axis normal to the gold/IL interface and the vector normal to the imidazolium ring (cf. Figure 5).

one centered at 90° (ring plane perpendicular to the gold surface) and two more peaks found at $\sim 10^\circ$ and $\sim 170^\circ$ which, due to symmetry considerations, represent the ring in a conformation close to parallel to the gold interface. The integration of the first and third peaks stopping or starting at its minimum shows that about 60% of $[\text{BMIm}]^+$ ions have the imidazolium rings in an orientation that is close to planar to the interface (this value is basically independent if the first minimum is defined at 45° and the second at 135° to consider the ring in a parallel orientation).

Ultrathin ionic liquid films of $[\text{C}_1\text{C}_1\text{Im}][\text{NTf}_2]$ (1-methyl-3-methylimidazolium bis(trifluoromethylsulfonyl)imide) and $[\text{C}_8\text{C}_1\text{Im}][\text{NTf}_2]$ (1-octyl-3-methylimidazolium bis(trifluoromethylsulfonyl)imide) adsorbed at Au(111) were studied by Steinrück and co-workers^{60,61} via angle-resolved X-ray photoelectron spectroscopy (ARXPS). The results showed that the cations in direct contact with gold have the imidazolium ring parallel to the surface. The $[\text{NTf}_2]^-$ anions are in a cis conformation with SO_2 groups pointing toward gold

and the CF_3 groups pointing toward the liquid. The global arrangement of the ions was proposed to be most likely a checkerboard-type arrangement in order to optimize charge neutrality. However, for the $[\text{C}8\text{C}1\text{Im}]$ a lower degree of ordering was found with the alkyl chains pointing away from the surface as the coverage increases. Uhl et al.⁶² studied by ARXPS other ionic liquid ($[\text{BMP}][\text{NTf}_2]$; 1-butyl-1-methylpyrrolidinium-bis(trifluoromethylsulfonyl)imide) also adsorbed at the Au(111) surface and having obtained similar results.

The final configuration of the production run for the $[\text{BMIm}][\text{NTf}_2]$ /gold system was used to extract the first layer in direct contact with gold. In Figure 11, the ions are

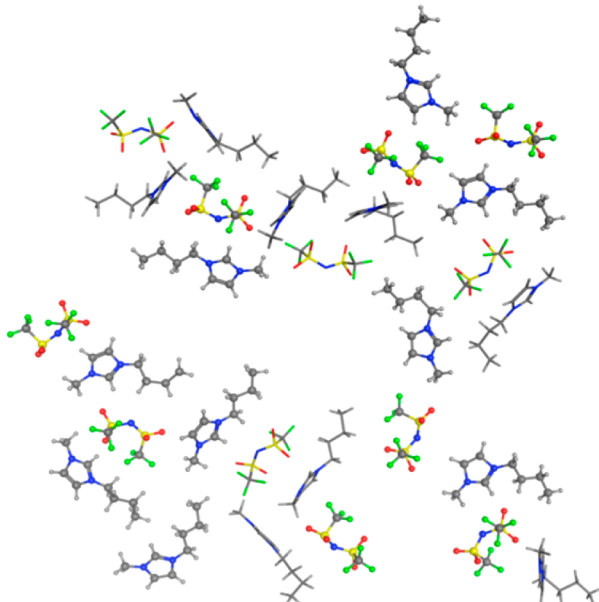


Figure 11. Final configuration of the production run for $[\text{BMIm}][\text{NTf}_2]$ gold system. The $[\text{BMIm}]^+$ ions with the imidazolium ring parallel to the interface and the $[\text{NTf}_2]^-$ anions with at least one $\text{S}-\text{CF}_3$ vector perpendicular to the interface are represented in CPK.

represented in different forms according to the orientation of the imidazolium ring (CPK representation means an orientation close to planar: 9 in 17 ions). For $[\text{NTf}_2]^-$ a CPK representation means that one $\text{S}-\text{CF}_3$ bond is oriented parallel and the other perpendicular to the interface (8 in 12 ions). This same final system configuration is also represented through van der Waals spheres in Figure 12. For clarity the gold atoms are not represented but are located just beneath the surface defined by the ions.

The system was replicated once in the x and y directions (interfacial plane), and the size of the interface is represented by the black square. Although the symmetry of the system can induce some degree of ordered repetition, it is clear from the figure that the ions are not randomly disposed on the surface with the anions arranged around the cations usually in the neighborhood of the imidazolium ring to induce charge neutrality at the subnanometer level. Nevertheless, the picture shows some degree of island formations even though the IL/gold surface has to be bigger for this type of macromolecular organization to be clearly perceived and studied.

CONCLUSIONS

Using classical molecular dynamic simulations, we studied the structure of two IL/gold interfaces, $[\text{BMIm}][\text{PF}_6]$ /gold and

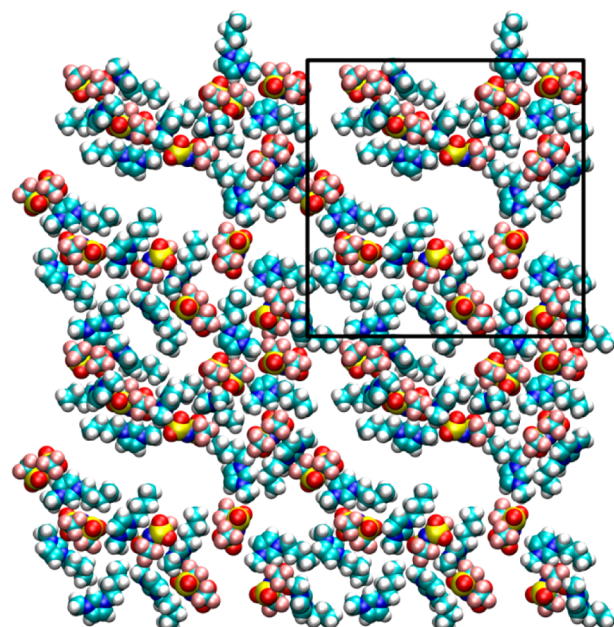


Figure 12. Final configuration of the production run for $[\text{BMIm}][\text{NTf}_2]$ gold system. The $[\text{BMIm}]^+$ and $[\text{NTf}_2]^-$ ions found in the first peak as defined by the density profiles found in Figure 1 are represented in vdW spheres. The carbon atoms are represented in light blue, nitrogen in dark blue, sulfur atoms in yellow, hydrogen atoms in white. For clarity the system is replicated once in the x and y directions, and the real interface size is represented by the black square.

$[\text{BMIm}][\text{NTf}_2]$ /gold. This study shows that there is a strong layering of the ions near the surface, especially in the first and second layers, with a higher layering effect for $[\text{BMIm}][\text{NTf}_2]$ and a higher packing capacity for $[\text{BMIm}][\text{PF}_6]$ ionic liquids. Thus, potential drops are higher for IL with the $[\text{PF}_6]^-$ anion, which is a smaller anion than $[\text{NTf}_2]^-$.

The distribution of orientations of the imidazolium rings in the first layer tends to be perpendicular to the gold surface in about 60% of the cases, while its alkyl side chain tends to be parallel to this interface, for both ILs. This shows that the molecular orientations have a higher dependency on the interface rather than on the anion. When considering the second layer of the cation, the orientation of these ions tend to be much more random, with no preferable orientation for rings or tails being discernible.

For the $[\text{NTf}_2]^-$ anions a parallel orientation for the S-S axis is observed (tilt axis defined by the vector uniting the two sulfur atoms), while for the two $\text{S}-\text{CF}_3$ axes they are either almost perpendicular or almost parallel to the interface. With respect to the $[\text{PF}_6]^-$ anions, there is a preference for one of the fluorine atoms to be in closer contact to gold.

Near the interface the anions are located around the cations, usually in the neighborhood of the imidazolium rings to induce charge neutrality, and there seems to be some degree of island formations.

This study provides important information to elucidate the role of molecule–surface and molecule–molecule interactions, and it comprises a basis for reaching a clear physical representation about these ionic liquids/gold interfaces. In future studies, we plan to investigate the EDL structure near a charged surface by using MD simulations.

AUTHOR INFORMATION

Corresponding Authors

*E-mail: cmpereir@fc.up.pt.
*E-mail: ncordeir@fc.up.pt.
*E-mail: ddsantos@fc.up.pt.

Notes

The authors declare no competing financial interest.

ACKNOWLEDGMENTS

This work received financial support from *Fundação para a Ciência e Tecnologia* (FCT, Lisbon, Portugal) through projects UID/QUI/50006/2013 and PEst-C/QUI/UI0081/2013 (LAQV@REQUIMTE and CIQUP, respectively). E.S.F. and D.J.V.A.d.S. thank also FCT for, respectively, the postdoctoral grant SFRH/BPD/90343/2012 cofunded by the European Social Fund and the Research Assistant contract funded within the Ciência2008 programme.

REFERENCES

- (1) Zhang, M.; Liang, X.; Jiang, S.; Qiu, H. Preparation and Applications of Surface-Confining Ionic-Liquid Stationary Phases For Liquid Chromatography. *TrAC, Trends Anal. Chem.* **2014**, *53*, 60–72.
- (2) Dale, P. J.; Samantilleke, A. P.; Shivagan, D. D.; Peter, L. M. Synthesis of Cadmium and Zinc Semiconductor Compounds from an Ionic Liquid Containing Choline Chloride and Urea. *Thin Solid Films* **2007**, *515*, 5751–5754.
- (3) Huddleston, J. G.; Visser, A. E.; Reichert, W. M.; Willauer, H. D.; Broker, G. A.; Rogers, R. D. Characterization and Comparison of Hydrophilic and Hydrophobic Room Temperature Ionic Liquids Incorporating the Imidazolium Cation. *Green Chem.* **2001**, *3*, 156–164.
- (4) Hallett, J. P.; Welton, T. Room-Temperature Ionic Liquids: Solvents for Synthesis and Catalysis. *2. Chem. Rev.* **2011**, *111*, 3508–3576.
- (5) Brennecke, J. F.; Gurkan, B. E. Ionic Liquids for CO₂ Capture and Emission Reduction. *J. Phys. Chem. Lett.* **2010**, *1*, 3459–3464.
- (6) Fedorov, M. V.; Kornyshev, A. A. Ionic Liquids at Electrified Interfaces. *Chem. Rev.* **2014**, *114*, 2978–3036.
- (7) Ferreira, E. S. C.; Pereira, C. M.; Silva, A. F. Electrochemical Studies of Metallic Chromium Electrodeposition from a Cr(III) Bath. *J. Electroanal. Chem.* **2013**, *707*, 52–58.
- (8) Salomé, S.; Pereira, N. M.; Ferreira, E. S.; Pereira, C. M.; Silva, A. F. Tin Electrodeposition from Choline Chloride Based Solvent: Influence of the Hydrogen Bond Donors. *J. Electroanal. Chem.* **2013**, *703*, 80–87.
- (9) Leones, R.; Costa, C. M.; Machado, A. V.; Esperança, J. M. S. S.; Silva, M. M.; Lanceros-Méndez, S. Development of Solid Polymer Electrolytes Based on Poly(vinylidene fluoride-trifluoroethylene) and the [N1 1 1 2(OH)][NTf₂]⁻ Ionic Liquid for Energy Storage Applications. *Solid State Ionics* **2013**, *253*, 143–150.
- (10) Hayes, R.; Borisenko, N.; Tam, M. K.; Howlett, P. C.; Endres, F.; Atkin, R. Double Layer Structure of Ionic Liquids at the Au(111) Electrode Interface: An Atomic Force Microscopy Investigation. *J. Phys. Chem. C* **2011**, *115*, 6855–6863.
- (11) Mohd Noor, S. A.; Howlett, P. C.; MacFarlane, D. R.; Forsyth, M. Properties of Sodium-Based Ionic Liquid Electrolytes for Sodium Secondary Battery Applications. *Electrochim. Acta* **2013**, *114*, 766–771.
- (12) Hantal, G.; Voroshlova, I.; Cordeiro, M. N. D. S.; Jorge, M. A. Systematic Molecular Simulation Study of Ionic Liquid Surfaces Using Intrinsic Analysis Methods. *Phys. Chem. Chem. Phys.* **2012**, *14*, S200–S213.
- (13) Hantal, G.; Cordeiro, M. N. D. S.; Jorge, M. What Does an Ionic Liquid Surface Really Look Like? Unprecedented Details from Molecular Simulations. *Phys. Chem. Chem. Phys.* **2011**, *13*, 21230–21232.
- (14) Lynden-Bell, R. M.; Frolov, A. I.; Fedorov, M. V. Electrode Screening by Ionic Liquids. *Phys. Chem. Chem. Phys.* **2012**, *14*, 2693–2701.
- (15) Vatamanu, J.; Borodin, O.; Smith, G. D. Molecular Insights into the Potential and Temperature Dependences of the Differential Capacitance of a Room-Temperature Ionic Liquid at Graphite Electrodes. *J. Am. Chem. Soc.* **2010**, *132*, 14825–14833.
- (16) Feng, G.; Qiao, R.; Huang, J.; Dai, S.; Sumpter, B. G.; Meunier, V. The Importance of Ion Size and Electrode Curvature on Electrical Double Layers in Ionic Liquids. *Phys. Chem. Chem. Phys.* **2011**, *13*, 1152–1161.
- (17) Alam, M. T.; Masud, J.; Islam, M. M.; Okajima, T.; Ohsaka, T. Differential Capacitance at Au(111) in 1-Alkyl-3-methylimidazolium Tetrafluoroborate Based Room-Temperature Ionic Liquids. *J. Phys. Chem. C* **2011**, *115*, 19797–19804.
- (18) Islam, M. M.; Alam, M. T.; Ohsaka, T. Electrical Double-Layer Structure in Ionic Liquids: A Corroboration of the Theoretical Model by Experimental Results. *J. Phys. Chem. C* **2008**, *112*, 16568–16574.
- (19) Alam, M. T.; Islam, M. M.; Okajima, T.; Ohsaka, T. Capacitance Measurements in a Series of Room-Temperature Ionic Liquids at Glassy Carbon and Gold Electrode Interfaces. *J. Phys. Chem. C* **2008**, *112*, 16600–16608.
- (20) Gnahn, M.; Pajkossy, T.; Kolb, D. M. The Interface between Au(111) and an Ionic Liquid. *Electrochim. Acta* **2010**, *55*, 6212–6217.
- (21) Gore, T. R.; Bond, T.; Zhang, W.; Scott, R. W. J.; Burgess, I. J. Hysteresis in the Measurement of Double-Layer Capacitance at the Gold–Ionic Liquid Interface. *Electrochim. Commun.* **2010**, *12*, 1340–1343.
- (22) Lockett, V.; Horne, M.; Sedev, R.; Rodopoulos, T.; Ralston, J. Differential Capacitance of the Double Layer at the Electrode/Ionic Liquids Interface. *Phys. Chem. Chem. Phys.* **2010**, *12*, 12499–12512.
- (23) Roling, B.; Drüscher, M.; Huber, B. Slow and Fast Capacitive Process Taking Place at the Ionic Liquid/Electrode Interface. *Faraday Discuss.* **2012**, *154*, 303–311.
- (24) Drüscher, M.; Huber, B.; Roling, B. On Capacitive Processes at the Interface between 1-Ethyl-3-methylimidazolium tris(pentafluoroethyl)trifluorophosphate and Au(111). *J. Phys. Chem. C* **2011**, *115*, 6802–6808.
- (25) Silva, F.; Gomes, C.; Figueiredo, M.; Costa, R.; Martins, A.; Pereira, C. M. The Electrical Double Layer at the [BMIM][PF₆] Ionic Liquid/Electrode Interface – Effect of Temperature on the Differential Capacitance. *J. Electroanal. Chem.* **2008**, *622*, 153–160.
- (26) Wang, S.; Li, S.; Cao, Z.; Yan, T. Molecular Dynamic Simulations of Ionic Liquids at Graphite Surface. *J. Phys. Chem. C* **2010**, *114*, 990–995.
- (27) Crozier, P. S.; Rowley, R. L.; Henderson, D. Molecular-Dynamics Simulations of Ion Size Effects on the Fluid Structure of Aqueous Electrolyte Systems between Charged Model Electrodes. *J. Chem. Phys.* **2001**, *114*, 7513–7517.
- (28) Tariq, M.; Forte, P. A. S.; Gomes, M. F. C.; Lopes, J. N. A. C.; Rebele, L. P. N. Densities and Refractive Indices of Imidazolium- and Phosphonium-Based Ionic Liquids: Effect of Temperature, Alkyl Chain Length, and Anion. *J. Chem. Thermodyn.* **2009**, *41*, 790–798.
- (29) Plechkova, N. V.; Seddon, K. R. Applications of Ionic Liquids in the Chemical Industry. *Chem. Soc. Rev.* **2008**, *37*, 123–150.
- (30) Shah, J. K.; Brennecke, J. F.; Maginn, E. J. Thermodynamic Properties of the Ionic Liquid 1-N-Butyl-3-Methylimidazolium Hexafluorophosphate from Monte Carlo Simulations. *Green Chem.* **2002**, *4*, 112–118.
- (31) Margulis, C. J.; Stern, H. A.; Berne, B. J. Computer Simulation of a “Green Chemistry” Room-Temperature Ionic Solvent. *J. Phys. Chem. B* **2002**, *106*, 12017–12021.
- (32) Morrow, T. I.; Maginn, E. J. Molecular Dynamics Study of the Ionic Liquid 1-n-Butyl-3-methylimidazolium Hexafluorophosphate. *J. Phys. Chem. B* **2002**, *106*, 12807–12813.
- (33) Wang, Y.; Voth, G. A. Unique Spatial Heterogeneity in Ionic Liquids. *J. Am. Chem. Soc.* **2005**, *127*, 12192–12193.
- (34) Canongia Lopes, J. N. A.; Pádua, A. A. H. Nanostructural Organization in Ionic Liquids. *J. Phys. Chem. B* **2006**, *110*, 3330–3335.

- (35) Triolo, A.; Russina, O.; Bleif, H.-J.; Di Cola, E. Nanoscale Segregation in Room Temperature Ionic Liquids. *J. Phys. Chem. B* **2007**, *111*, 4641–4644.
- (36) Xiao, D.; Rajian, J. R.; Cady, A.; Li, S.; Bartsch, R. A.; Quitevis, E. L. Nanostructural Organization and Anion Effects on the Temperature Dependence of the Optical Kerr Effect Spectra of Ionic Liquids. *J. Phys. Chem. B* **2007**, *111*, 4669–4677.
- (37) Zhang, X.; Zhong, Y.-X.; Yan, J.-W.; Su, Y.-Z.; Zhang, M.; Mao, B.-W. Probing Double Layer Structures of Au (111)-BMIPF6 Ionic Liquid Interfaces from Potential-Dependent AFM Force Curves. *Chem. Commun.* **2012**, *48*, 582–584.
- (38) Sha, M.; Wu, G.; Dou, Q.; Tang, Z.; Fang, H. Double-Layer Formation of [Bmim][PF6] Ionic Liquid Triggered by Surface Negative Charge. *Langmuir* **2010**, *26*, 12667–12672.
- (39) Molecular Operating Environment (MOE), 2013.08; Chemical Computing Group Inc., 1010 Sherbooke St. West, Suite #910, Montreal, QC, Canada, H3A 2R7, 2015.
- (40) Dos Santos, D. J. V. A.; Cordeiro, M. N. D. S. Effect of Replacing [Ntf2] By [PF6] Anion on the [Bmim][Ntf2] Ionic Liquid Confined by Gold. *Mol. Simul.* **2015**, *41*, 455–462.
- (41) Heinz, H.; Vaia, R. A.; Farmer, B. L.; Naik, R. R. Accurate Simulation of Surfaces and Interfaces of Face-Centered Cubic Metals Using 12-6 and 9-6 Lennard-Jones Potentials. *J. Phys. Chem. C* **2008**, *112*, 17281–17290.
- (42) Canongia Lopes, J. N.; Deschamps, J.; Pádua, A. A. H. Modeling Ionic Liquids Using a Systematic All-Atom Force Field. *J. Phys. Chem. B* **2004**, *108*, 2038–2047.
- (43) Köddermann, T.; Paschek, D.; Ludwig, R. Molecular Dynamic Simulations of Ionic Liquids: A Reliable Description of Structure, Thermodynamics and Dynamics. *ChemPhysChem* **2007**, *8*, 2464–2470.
- (44) Hess, B.; Kutzner, C.; van der Spoel, D.; Lindahl, E. GROMACS 4: Algorithms for Highly Efficient, Load-Balanced, and Scalable Molecular Simulation. *J. Chem. Theory Comput.* **2008**, *4*, 435–447.
- (45) Darden, T.; York, D.; Pedersen, L. Particle Mesh Ewald: An N-Log(N) Method for Ewald Sums in Large Systems. *J. Chem. Phys.* **1993**, *98*, 10089–10092.
- (46) Essmann, U.; Perera, L.; Berkowitz, M. L.; Darden, T.; Lee, H.; Pedersen, L. G. A Smooth Particle Mesh Ewald Method. *J. Chem. Phys.* **1995**, *103*, 8577–8593.
- (47) Nosé, S. A Molecular Dynamics Method for Simulations in the Canonical Ensemble. *Mol. Phys.* **1984**, *52*, 255–268.
- (48) Hoover, W. G. Canonical Dynamics: Equilibrium Phase-Space Distributions. *Phys. Rev. A: At., Mol., Opt. Phys.* **1985**, *31*, 1695–1697.
- (49) Parrinello, M.; Rahman, A. Polymorphic Transitions in Single Crystals: A New Molecular Dynamics Method. *J. Appl. Phys.* **1981**, *52*, 7182–7190.
- (50) Rocha, M. A. A.; Ribeiro, F. M. S.; Ferreira, A. I. M. C. L.; Coutinho, J. A. P.; Santos, L. M. N. B. F. Thermophysical Properties of [CN-1-C1im][PF6] Ionic Liquids. *J. Mol. Liq.* **2013**, *188*, 196–202.
- (51) Rocha, M. A. A.; Neves, C. M. S. S.; Freire, M. G.; Russina, O.; Triolo, A.; Coutinho, J. A. P.; Santos, L. M. N. B. F. Alkylimidazolium Based Ionic Liquids: Impact of Cation Symmetry on Their Nanoscale Structural Organization. *J. Phys. Chem. B* **2013**, *117*, 10889–10897.
- (52) Si, X.; Li, S.; Wang, Y.; Ye, S.; Yan, T. Effects of Specific Adsorption on the Differential Capacitance of Imidazolium-Based Ionic Liquid Electrolytes. *ChemPhysChem* **2012**, *13*, 1671–1676.
- (53) Liu, X.; Han, Y.; Yan, T. Temperature Effects on the Capacitance of an Imidazolium-based Ionic Liquid on a Graphite Electrode: A Molecular Dynamics Simulation. *ChemPhysChem* **2014**, *15*, 2503–2509.
- (54) Jin, W.; Liu, X.; Han, Y.; Li, S.; Yan, T. Effects of Repulsive Interaction on the Electric Double Layer of an Imidazolium-Based Ionic Liquid by Molecular Dynamics Simulation. *Phys. Chem. Chem. Phys.* **2015**, *17*, 2628–2633.
- (55) Kislenko, S. A.; Amirov, R. H.; Samoylov, I. S. Molecular Dynamics Simulation of the Electrical Double Layer in Ionic Liquids. *J. Phys.: Conf. Ser.* **2013**, *418*, 012021.
- (56) Pratt, L. R. Contact Potentials of Solution Interfaces - Phase-Equilibrium and Interfacial Electric-Fields. *J. Phys. Chem.* **1992**, *96*, 25–33.
- (57) Fernandes, P. A.; Cordeiro, M. N. D. S.; Gomes, J. A. N. F. Molecular Simulation of the Interface between Two Immiscible Electrolyte Solutions. *J. Phys. Chem. B* **2001**, *105*, 981–993.
- (58) Vatamanu, J.; Borodin, O.; Bedrov, D.; Smith, G. D. Molecular Dynamics Simulation Study of the Interfacial Structure and Differential Capacitance of Alkylimidazolium Bis (trifluoromethanesulfonyl) imide [C_nmim][TFSI] Ionic Liquids at Graphite Electrodes. *J. Phys. Chem. C* **2012**, *116*, 7940–7951.
- (59) Li, S.; Feng, G.; Cummings, P. T. Interfaces of Dicationic Ionic Liquids and Graphene: A Molecular Dynamics Simulation Study. *J. Phys.: Condens. Matter* **2014**, *26*, 284106.
- (60) Cremer, T.; Stark, M.; Deyko, A.; Steinrück, H. P.; Maier, F. Liquid/Solid Interface of Ultrathin Ionic Liquid Films: [C1C1Im]-[Tf2N] and [C8C1Im]-[Tf2N] on Au(111). *Langmuir* **2011**, *27*, 3662–3671.
- (61) Steinrück, H.-P. Recent Developments in the Study of Ionic Liquid Interfaces Using X-Ray Photoelectron Spectroscopy and Potential Future Directions. *Phys. Chem. Chem. Phys.* **2012**, *14*, 5010–5029.
- (62) Uhl, B.; Cremer, T.; Roos, M.; Maier, F.; Steinrück, H.-P.; Behm, R. J. At the Ionic Liquid/Metal Interface: Structure Formation and Temperature Dependent Behavior of an Ionic Liquid Adlayer on Au(111). *Phys. Chem. Chem. Phys.* **2013**, *15*, 17295–17302.